Cell Metabolism
Article

Glucose Utilization via Glycogen Phosphorylase Sustains Proliferation and Prevents Premature Senescence in Cancer Cells

Elena Favaro,[1] Karim Bensaad,[1] Mei G. Chong,[2] Daniel A. Tennant,[2] David J.P. Ferguson,[3] Cameron Snell,[3] Graham Steers,[3] Helen Turley,[3] Ji-Liang Li,[1] Ulrich L. Günther,[2] Francesca M. Buffa,[1] Alan McIntyre,[1] and Adrian L. Harris[1,*]

[1]Molecular Oncology Laboratories, Weatherall Institute of Molecular Medicine, University of Oxford, John Radcliffe Hospital, Oxford OX3 9DS, UK

[2]School of Cancer Sciences, University of Birmingham, Birmingham B15 2TT, UK

[3]Nuffield Department of Clinical Laboratory Sciences, University of Oxford, John Radcliffe Hospital, Oxford OX3 9DU, UK

*Correspondence: adrian.harris@oncology.ox.ac.uk

http://dx.doi.org/10.1016/j.cmet.2012.10.017

SUMMARY

Metabolic reprogramming of cancer cells provides energy and multiple intermediates critical for cell growth. Hypoxia in tumors represents a hostile environment that can encourage these transformations. We report that glycogen metabolism is upregulated in tumors in vivo and in cancer cells in vitro in response to hypoxia. In vitro, hypoxia induced an early accumulation of glycogen, followed by a gradual decline. Concordantly, glycogen synthase (GYS1) showed a rapid induction, followed by a later increase of glycogen phosphorylase (PYGL). PYGL depletion and the consequent glycogen accumulation led to increased reactive oxygen species (ROS) levels that contributed to a p53-dependent induction of senescence and markedly impaired tumorigenesis in vivo. Metabolic analyses indicated that glycogen degradation by PYGL is important for the optimal function of the pentose phosphate pathway. Thus, glycogen metabolism is a key pathway induced by hypoxia, necessary for optimal glucose utilization, which represents a targetable mechanism of metabolic adaptation.

INTRODUCTION

A fundamental property of cancer cells is that they undergo metabolic reprogramming in response to the hypoxic environment present in solid tumors. Cancer cells rely primarily on aerobic glycolysis to sustain their proliferation (Lunt and Vander Heiden, 2011). The increased uptake and metabolism of glucose even in the presence of oxygen is known as the "Warburg effect" (Warburg, 1956). This is a relatively inefficient way to generate ATP (2 ATPs per glucose) as compared to oxidative phosphorylation (36 ATPs per glucose), and it contributes to only 17% of the total ATP production (Zu and Guppy, 2004), suggesting other critical roles for aerobic glycolysis. Indeed, many observations have proposed a role for glycolysis in providing precursors for anabolic pathways (e.g., lipids, nucleotides, and amino acids), as well as cofactors (e.g., NADH and NADPH), which are required for cancer cell proliferation (Ward and Thompson, 2012). To address the effect of the hypoxic microenvironment on metabolic pathways, we used an in vivo model in which xenografts of U87 glioblastoma cells were treated with the antiangiogenic drug bevacizumab, and the gene expression profile was compared to untreated tumors. Several established HIF-targets (including CA9 [Wykoff et al., 2000]) were upregulated, reflecting the increase in intratumoral hypoxia. Moreover, numerous metabolic pathways were modulated. One of these was glycogen metabolism.

Glycogen comprises a store of glucose, which is mainly present in liver and muscles. The structure consists of long polymeric chains of glucose units linked by alpha (α)-1,4 glycosidic bonds with occasional α-1,6 glycosidic bonds that generate branching points and increase solubility (Berg et al., 2002). Synthesis and breakdown of glycogen involves the activity of several enzymes and regulatory proteins. Among these, glycogen synthase (GS) and glycogen phosphorylase (GP) catalyze the key steps of synthesis and degradation, respectively (see Figure S1A online) (Berg et al., 2002). GS elongates glycogen branches through the formation of α-1,4 glycosidic bridges, whereas GP cleaves these, releasing glucose-1-phosphate (G1P) that can enter the glycolytic pathway or the pentose phosphate pathway (PPP) by conversion to glucose-6-phosphate (G6P). GS has two isoforms: GYS1 (muscle) and GYS2 (liver) (Roach et al., 1998). GP has three: PYGM (muscle), PYGL (liver), and PYGB (brain) (Newgard et al., 1989). The activity of these enzymes can be modulated by posttranslational modification (e.g., phosphorylation, stimulated by the hormones glucagon and epinephrine, which have inhibitory and activating effects on GS and GP, respectively) and allosteric effectors (ATP, AMP, and G6P) (Johnson, 1992; Lawrence and Roach, 1997).

A number of observations have suggested that the turnover of glycogen is altered in tumor cells. The levels of glycogen were demonstrated to be particularly high in breast, kidney, uterus, bladder, ovary, skin, and brain cancer cell lines. Glycogen content in these cells was inversely correlated with proliferation

rate (Rousset et al., 1981). Glycogen accumulation under hypoxic conditions has also been observed in several noncancer and cancer cell lines (Mamedova et al., 2003; Pelletier et al., 2012; Pescador et al., 2010; Shen et al., 2010; Vigoda et al., 2003). Consistent with these observations, GYS1 and other proteins involved in glycogen synthesis are induced in hypoxia in a HIF1α-dependent manner (Mole et al., 2009; Pelletier et al., 2012; Pescador et al., 2010; Shen et al., 2010). *PYGL* was included in a list of 99 genes defining the hypoxia "metagene," a signature defined in vivo in head and neck squamous cell carcinomas (HNSCCs) by clustering genes with similar expression patterns to that of well-characterized hypoxia-regulated genes (Winter et al., 2007). This signature proved to be prognostic in independent HNSCC and breast cancer series.

Recent studies have suggested a critical role of glycogen in promoting the survival of cancer cells. In particular, it has been demonstrated that a small molecule inhibitor of glycogen breakdown could induce apoptosis in pancreatic tumor cells (Lee et al., 2004). Furthermore, it has been shown by two independent studies that glycogen accumulation in cancer cells improves survival in response to low oxygen concentration and glucose deprivation (Pelletier et al., 2012; Pescador et al., 2010). Taken together, these observations suggested a role for glycogen in promoting tumor growth in hypoxic environments.

In this study, we further characterized the roles of glycogen-metabolizing enzymes in cancer cell biology. We demonstrate that glycogen levels undergo dramatic temporal changes in cancer cells exposed to hypoxic stress. Furthermore, we show that PYGL depletion (and consequent glycogen accumulation) induces premature senescence via a ROS-dependent mechanism, reduces the input into the PPP, and strongly impairs tumor growth. Surprisingly, glucose utilization via glycogen, rather than direct entry into downstream pathways, is necessary for optimum growth. Our study reveals an important contribution of glycogen metabolism to cancer cell proliferation, survival, and free radical protection in the context of metabolic reprogramming.

RESULTS

Glycogen-Metabolizing Genes Are Upregulated by Antiangiogenic Treatment

We focused our analyses on U87 (glioblastoma), MCF-7 (breast), and HCT116 (colon) cancer cell lines, as previous studies have shown elevated levels of glycogen in these cell lines (Rousset et al., 1981). To further identify the metabolic pathways required for the survival of tumor cells in hypoxic environments, we analyzed the gene expression profile of xenografts of the glioblastoma cell line U87 treated with the VEGF inhibitor bevacizumab. After chronic administration of bevacizumab, these tumors were characterized by regrowth and development of resistance to the treatment.

We observed that carbonic anhydrase IX (*CA9*), which is an indicator of HIF1α activation (Wykoff et al., 2000), was upregulated in bevacizumab-treated tumors, as compared to control tumors (Figure 1A). A number of genes implicated in glycogen metabolism (e.g., protein phosphatase 1, regulatory subunit 3B [*PPP1R3B*]; glycogen synthase 1 [*GYS1*]; acid α-glucosidase [*GAA*]; protein phosphatase 1, regulatory subunit 3C [*PPP1R3C*]; liver glycogen phosphorylase [*PYGL*]; glycogen branching enzyme 1 [*GBE1*]; Genethonin-1 [*GENX-3414*]; and phosphoglucomutase 1 [*PGM1*]) were similarly upregulated (Figure 1A and Figure S1A). The expression of *GYS1* and *PYGL*, which encode for the two main enzymes implicated in glycogen storage (GYS1) and breakdown (PYGL), were increased by 4.1- and 2.6-fold, respectively. We therefore focused our analyses on GYS1 and PYGL because of their central roles in glycogen metabolism. Increased expression of *CA9*, *GYS1*, and *PYGL* was confirmed at the mRNA level by RT-PCR (Figure 1B). Staining of serial sections revealed an increase in levels of the hypoxia marker pimonidazole (30.6% ± 4% versus 12.7% ± 3.9%), GYS1 (27.8% ± 1.4% versus 14.3% ± 3.7%), PYGL (69.9% ± 7% versus 37.7% ± 7.2%) and more than a 10-fold increase in glycogen, as detected by Periodic Acid-Schiff (PAS) staining (5.3% ± 2% versus 0.4% ± 0.2%) in bevacizumab-treated tumors (Figure S1B). A positive correlation between glycogen levels and hypoxia was also supported by colocalization of CA9 and PAS staining in the perinecrotic area of treated tumors (Figure 1C). Moreover, immunohistochemical analysis of HCT116 spheroids revealed that GYS1 and PYGL staining was more pronounced in (pimonidazole-positive) hypoxic cells (Figure 1D). Collectively, these results indicate that glycogen metabolism increases with hypoxia in tumors and spheroids.

Hypoxia Induces the Expression of *GYS1* and *PYGL* and Causes Characteristic Changes in Glycogen Metabolism

To further investigate the roles of GYS1 and PYGL and their association with hypoxia, we examined their expression in cancer cell lines cultivated in vitro. Analysis of *GYS1* and *PYGL* expression in U87 cells revealed distinct patterns of induction by hypoxia (0.1% O_2) that were consistent at both the mRNA (Figure 2A) and protein level (Figure 2B). We observed that *GYS1* levels increased rapidly in hypoxia, and then declined by 72 hr, whereas *PYGL* levels increased more slowly in hypoxia, and reached maximal levels at 72 hr. These findings were also confirmed in MCF-7 and HCT116 cell lines (Figures S2A and S2B). Glycogen synthesis through GYS1 requires intracellular availability of the allosteric activator G6P (Bouskila et al., 2010). We observed hypoxic induction of the glucose transporter GLUT1 and the glucose-phosphorylating enzyme hexokinase II (HKII) (Figure 2B), both of which have been previously characterized as HIF-target genes (Semenza, 2002). GYS1 is inhibited by phosphorylation (Lawrence and Roach, 1997); therefore, protein activity can be measured by comparing the ratio of phosphorylated:nonphosphorylated GYS1. Interestingly, we observed that after an initial decrease (12 hr), the level of phosphorylated GYS1 increased after 24 hr in hypoxia and remained constant from 24 to 72 hr in hypoxia, despite a time-dependent decrease in total GYS1 levels (Figure 2B). This suggests that a higher proportion of GYS1 is phosphorylated/inactivated in hypoxia at later time points.

We note that two other isoforms of PYGL also exist in human cells, PYGM and PYGB. However, we observed that, unlike *PYGL*, neither of these genes exhibited a detectable/significant hypoxia-induced increase in U87 cells (data not shown). Therefore, PYGL was likely to be the main GP activity required for glycogen breakdown in hypoxic cells.

A

Symbol	Description	Accession	Unigene	Fold change	Q value (%)
CA9	carbonic anhydrase IX	NM_001216	Hs.63287	11.2	0
PPP1R3B	protein phosphatase 1, regulatory subunit 3B	NM_024607	Hs.458513	4.2	0
GYS1	glycogen synthase 1	NM_002103	Hs.386225	4.1	0.2
GAA	acid α-glucosidase	NM_000152	Hs.1437	4.1	0.4
PPP1R3C	protein phosphatase 1, regulatory subunit 3C	N26005	Hs.303090	3.7	0
PYGL	phosphorylase, glycogen, liver	AU157823	Hs.282417	2.6	2.1
GBE1	glycogen branching enzyme 1	NM_024607	Hs.436062	2.1	0
GENX-3414	genethonin-1	NM_003943	Hs.109590	1.9	0.1
PGM1	phosphoglucomutase 1	NM_002633	Hs.1869	1.3	1.2

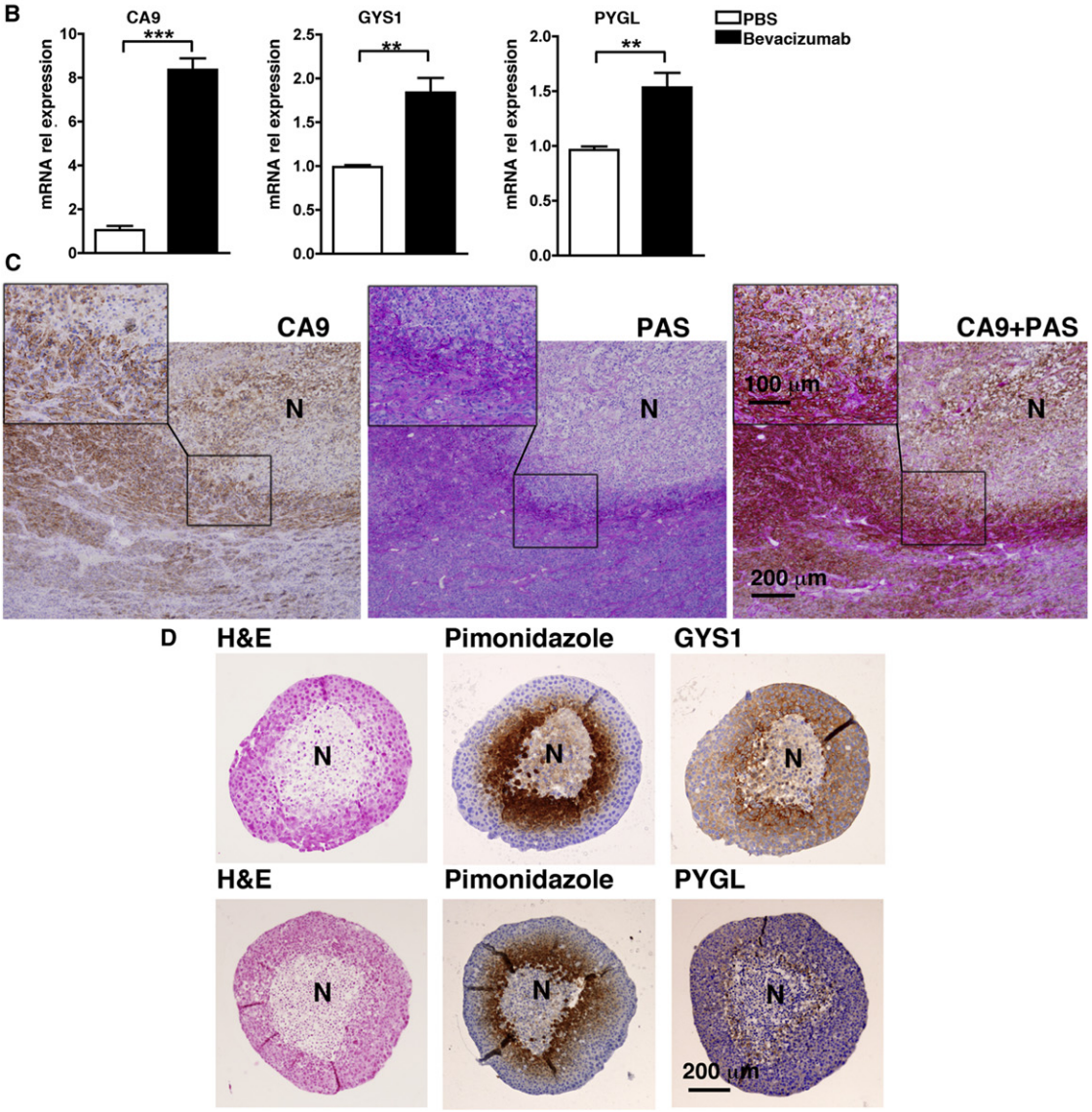

Figure 1. Glycogen Metabolism Is Modulated after Bevacizumab Treatment

(A) List of genes involved in glycogen metabolism, found to be upregulated in U87 xenografts treated with bevacizumab compared to controls.

(B) RT-PCR for CA9, GYS1, and PYGL in U87 xenografts treated with bevacizumab. Relative expression of GYS1 and PYGL is normalized to β-actin. Mean expression ± SEM in four animals/group is shown (**$p < 0.01$, ***$p < 0.001$).

(C) Serial sections derived from bevacizumab-treated U87 xenografts were stained for CA9 (left panel) and glycogen (PAS, middle panel) and costained for CA9 and glycogen (right panel). Two different magnifications are shown. N, necrosis.

(D) Haematoxylin and eosin (H&E) staining (left panels), and immunohistochemical staining of HCT116-derived spheroid. Serial sections were stained for pimonidazole (middle panels), GYS1 (top right panel), or PYGL (bottom right panel). N, necrosis. See also Figure S1.

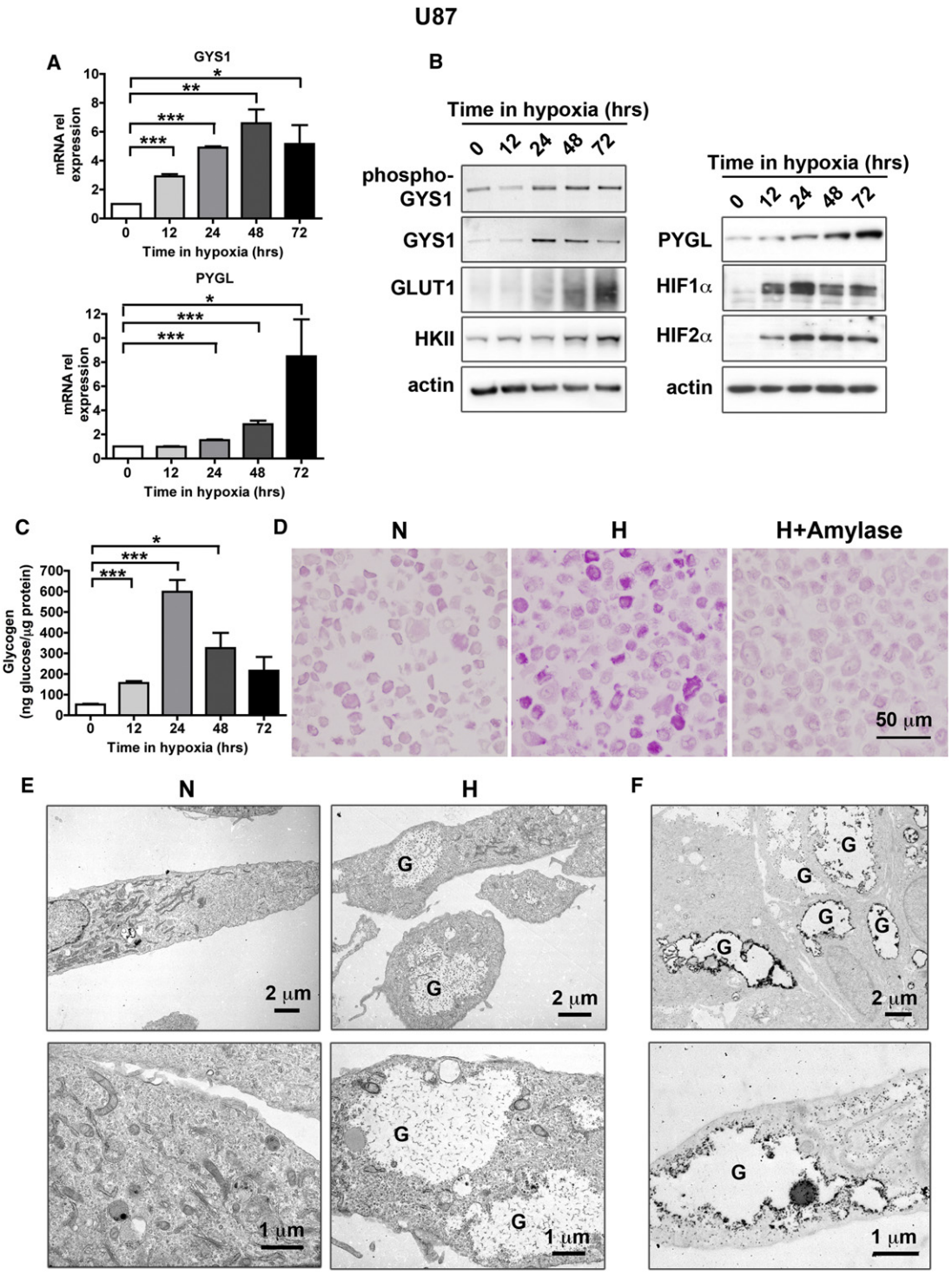

Figure 2. Pattern of GYS1 and PYGL Induction and Changes on Glycogen Level under Hypoxia

(A and B) In U87 cells, GYS1 expression is induced rapidly (12 hr) in hypoxia and starts to decrease at the later time points (72 hr), whereas PYGL expression follows a more delayed pattern of induction, with maximal expression at the later time points (72 hr). Shown are mRNA levels (A) and protein expression by immunoblotting (B) after 0, 12, 24, 48, or 72 hr in hypoxia. Levels of GYS1 and PYGL mRNA under hypoxia are relative to their levels at 0 hr. Mean ± SEM of three independent experiments is shown (*$p < 0.05$, **$p < 0.01$, ***$p < 0.001$). (C) Glycogen accumulation in hypoxia was measured by enzymatic assay in U87 cells exposed to hypoxia in a time course experiment. Glycogen was normalized by protein content. Mean ± SEM of three independent experiments is shown (*$p < 0.05$, ***$p < 0.001$). PAS staining (D) showing strong staining in the hypoxia-treated section, confirmed to be glycogen by the absence of staining after amylase pretreatment, and TEM (E) showing lucent pools of glycogen (G) in the hypoxic cells. U87 were exposed to hypoxia for 48 hr. N, normoxia; H, hypoxia. (F) Glycogen accumulation (G) was detected by specific staining for polysaccharides using an adaptation of the PATO method. See also Figures S2 and S3.

We observed that glycogen levels underwent a rapid increase, which peaked by 24 hr (598 ± 57 versus 52 ± 3 ng [glucose]/μg [protein]), and then gradually declined by 72 hr (216 ± 67 ng/μg) (Figure 2C). A similar pattern of glycogen metabolism alteration was also detected in MCF-7 cells (Figure S2C). Increased glycogen levels after 48 hr incubation of U87 cells in hypoxia were also confirmed by PAS staining and by transmission electron microscopy (TEM) (Figures 2D and 2E). TEM staining for polysaccharide material using the periodic acid-thiocarbohydrazide-osmium tetroxide (PATO) method (Ferguson et al., 1977) revealed electron-dense stain deposits both within and at the periphery of the irregular-shaped cytoplasmic structures, confirming that the lucent structures observed by routine electron microscopy contain glycogen (Figure 2F). Furthermore, similar structures were observed by TEM, when glycogen synthesis was induced in U87 cells with a glycogen synthase kinase 3 (GSK3) inhibitor (CHIR99021) (Ring et al., 2003) (Figure S2D).

Hypoxic induction of other glycogen metabolism enzymes (e.g., GAA and GBE) and regulatory proteins (e.g., PPP1R3B and PPP1R3C) identified from our initial analysis of bevacizumab-treated tumors (Figure 1A) was also confirmed in U87 cells by qPCR (Figure S2E). In particular, the lysosomal glycogenolytic GAA enzyme mRNA levels peaked at 72 hr, similarly to PYGL, whereas the branching enzyme GBE and the glycogenic proteins PPP1R3B and PPP1R3C exhibited an initial rapid increase in mRNA levels, followed by a decline by 72 hr, similar to what was observed for GYS1 induction.

To test the possibility that glycogen accumulation in hypoxia could be a consequence of the high glucose concentration (25 mM) present in standard culture media, we examined the consequences of lowering the glucose concentration to physiological blood levels (5 mM). We observed a pattern of GYS1 and PYGL induction and glycogen accumulation similar to that observed in high-glucose conditions in U87 cells (Figure S2F). Therefore, glycogen accumulation in hypoxia is not simply a consequence of high extracellular glucose concentration.

The hypoxic induction of GYS1 and PYGL led us to investigate the contribution of HIF1α. HIF-dependent regulation was evaluated in U87 and MCF-7 cells at the peak of hypoxic induction (48 hr for *GYS1* mRNA and 72 hr for *PYGL* mRNA [Figures 2A and 2B, Figure S2A]). In agreement with recent reports (Mole et al., 2009; Pescador et al., 2010), we observed that HIF1α depletion in U87 and MCF-7 cells prevented GYS1 induction in hypoxia (Figures S3A and S3B). Conversely, HIF-dependent induction of PYGL was not consistently observed in these cell lines and probably occurs indirectly in MCF-7 cells (Figures S3A and S3B). A previous report on genome-wide analysis of HIFα DNA binding in MCF-7 cells using chromatin immunoprecipitation did not reveal any *PYGL* promoter binding (Mole et al., 2009). These findings suggest that PYGL induction in hypoxia is unlikely to be HIF dependent.

PYGL Is Upregulated in Several Cancer Types

PYGL is one of the 99 genes defining the hypoxia "metagene," a gene signature derived from HNSCC, with poor prognostic outcome both in HNSCC and breast cancer (Winter et al., 2007). The Oncomine website (https://www.oncomine.org/) was queried for microarrays containing *PYGL*. A meta-analysis on over 2,000 cases showed that *PYGL* is upregulated in several cancer types, including clear cell renal carcinoma, papillary renal cell carcinoma, seminoma, and brain cancer (Figures S4A and S4B, Table S1), as compared to normal tissues. Furthermore, none of the studies examined thus far exhibited any downregulation of *PYGL*. Taken together, these findings suggested that the study of PYGL functions in hypoxia could have important clinical considerations. To analyze the levels of PYGL during various stages of tumor development, we utilized the Her-2/neu transgenic mouse model of breast cancer. In this model, the expression of neu, the rat homolog of the epidermal growth factor receptor Her-2, is controlled by the mouse mammary tumor virus-long terminal repeat (MMTV-LTR) promoter. These transgenic mice develop tumors that are morphologically similar to human ductal breast carcinomas (Ursini-Siegel et al., 2007). We therefore analyzed four tumor samples of different size (4, 6, 8, and 10 mm diameter) as representative tumors at different stages of development. Increased PYGL levels, as detected by immunostaining, were associated with increased tumor size, suggesting that PYGL is associated with tumor progression (Figure S4C).

PYGL Knockdown Is Associated with Glycogen Accumulation and Premature Senescence

To analyze the consequences of PYGL depletion in tumor cells, we then generated transient or stable PYGL knockdown U87 cells using RNA interference (RNAi). For this, we utilized multiple RNA sequences, each directed against a different site of the *PYGL* transcript. In both cases, the hypoxic induction of PYGL was prevented (Figure S4D), and this was associated with more pronounced glycogen accumulation in hypoxia (Figure 3A). Importantly, GYS1 levels were unaffected by PYGL knockdown (Figure 3B), suggesting that glycogen accumulation after 48 and 72 hr was a direct consequence of PYGL depletion. The accumulation of glycogen was also confirmed at 48 hr by measuring incorporation of the fluorescent glucose analog 2-NBDG into glycogen granules, by PAS staining, and by TEM (Figure 3C).

Depletion of PYGL was also associated with a significant reduction of U87 cell numbers after 48–72 hr exposure to hypoxia (Figure 4A). Furthermore, we verified that PYGL knockdown increased glycogen content and inhibited cell growth in the presence of lower (5 mM) glucose, confirming the physiological relevance of our findings (Figure S4E). The effects of PYGL knockdown were also confirmed by decreased clonogenic survival in MCF-7 cells under hypoxia (70.2% ± 4.1% compared to control in hypoxia) (Figure S4F). We note that PYGL depletion causes similar, albeit milder, effects in normoxic cells (Figure S4G). We conclude that PYGL depletion causes glycogen accumulation and decreased growth rate of cancer cell lines, and this phenotype is exacerbated in hypoxia.

To investigate the mechanism underlying this growth defect, we analyzed the effects of PYGL knockdown on cell viability. Analysis of Annexin V-positive cells and PARP cleavage showed only a minimal effect, suggesting that PYGL-depleted cells did not undergo apoptosis (Figure S4H). Analysis of the cell-cycle profile after PYGL knockdown in U87 cells revealed a higher proportion of cells in G1 phase with concomitant decreases in both S phase and G2/M phase, as compared to control cells (Figure 4B). This was associated with increased levels of the

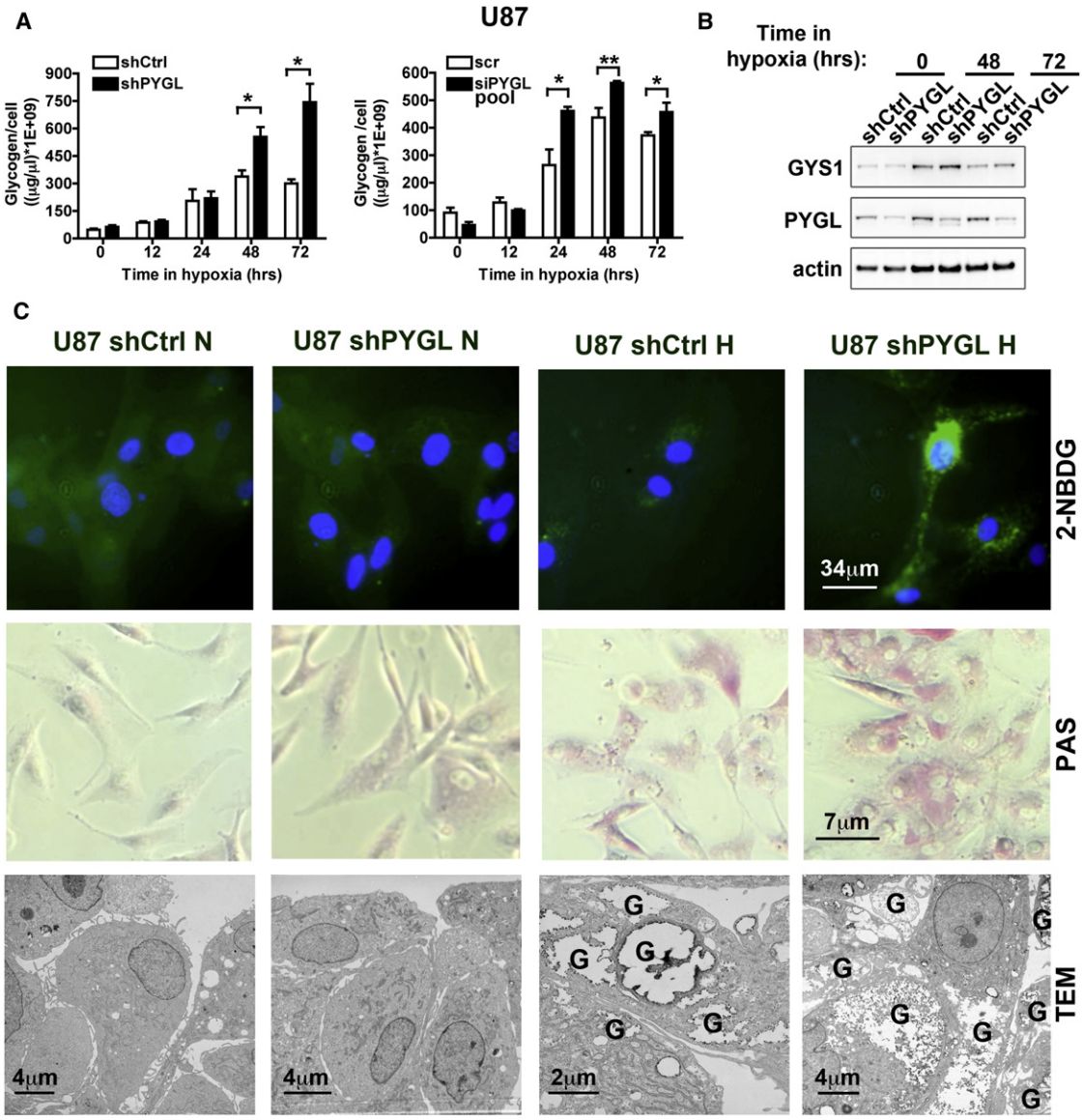

Figure 3. PYGL Knockdown Results in Glycogen Accumulation

(A) U87 were exposed to hypoxia in a time course experiment. Depletion of PYGL showed increased accumulation of glycogen compared to control after 48 and 72 hr in U87 shPYGL cells and after 24, 48, and 72 hr in U87 siPYGL pool cells. Glycogen content was normalized by cell number. Mean ± SEM of three independent experiments is shown (*$p < 0.05$, **$p < 0.01$).

(B) GYS1 protein is similarly expressed in U87 shCtrl and shPYGL cells after 48 or 72 hr in hypoxia.

(C) Glycogen accumulation in PYGL knockdown and control cells exposed to 0.1% O_2 for 48 hr was detected with the green fluorescent dye 2-NBDG (top panels), PAS staining (middle panels), and TEM (bottom panels). G, glycogen. See also Figure S4.

cell-cycle regulator p53 and its downstream target p21 (el-Deiry et al., 1993) (Figure 4C). To test if p53 induction was responsible for the decreased growth rate caused by PYGL knockdown, we investigated the effects of simultaneously depleting PYGL and p53. Knockdown of p53 prevented the decreased growth rate phenotype normally associated with PYGL depletion (Figures 4C and 4D).

Following PYGL depletion, U87 cells underwent characteristic morphological changes (i.e., enlargement and flattening) that were indicative of cellular senescence (Figure 5A). In addition to a G1 cell-cycle arrest, and increased levels of p53 and p21 (Figures 4B and 4C), increased expression of DEC1 (Collado et al., 2005; Schmitt, 2007) and an increased activity of senescence-associated β-galactosidase (SA β-gal), which correlates with an increase in lysosomal content (Kurz et al., 2000; Schmitt, 2007), have also been reported to be well-established markers for cellular senescence. Following PYGL knockdown, we observed an increase in both DEC1 and SA β-gal staining (Figures 5B and 5C and Figure S4I). After staining the cells with LysoTracker red, a dye that is selectively incorporated into

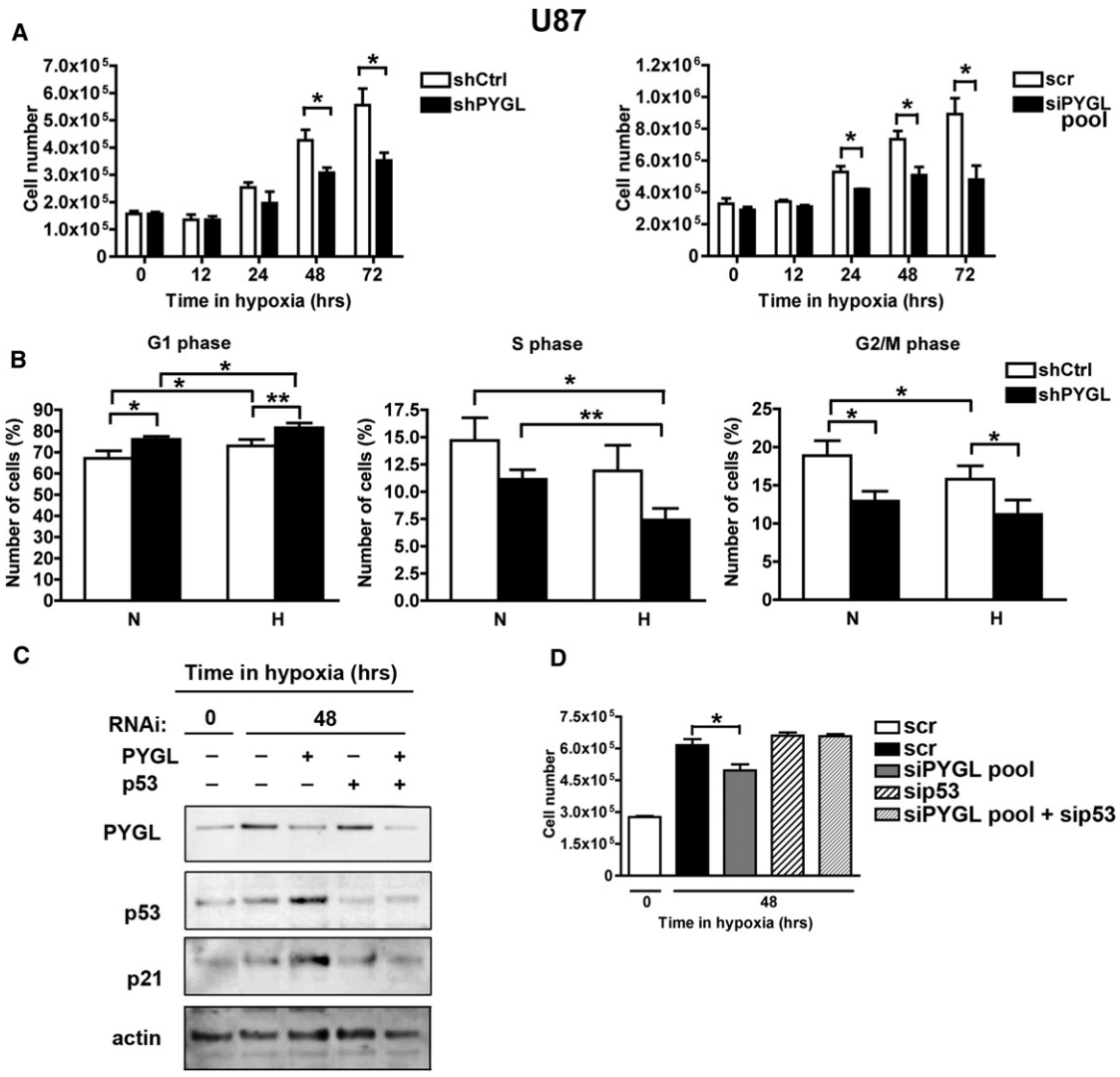

Figure 4. PYGL Sustains Proliferation in Cancer Cell Lines

(A) PYGL knockdown in U87 cells resulted in reduction of proliferation after 48 hr (shPYGL) or 24 hr (siPYGL pool) in hypoxia. Mean ± SEM of three independent experiments is shown (*$p < 0.05$).

(B) PYGL depletion in U87 cells was associated with increased G1 phase and decreased S and G2/M phases of the cell cycle. Cells were cultivated in normoxia (N) or hypoxia (H) for 48 hr. Mean ± SEM of three independent experiments is shown (*$p < 0.05$, **$p < 0.01$).

(C) Immunoblotting for the cell-cycle regulators p21 and p53 revealed increased levels after PYGL depletion at 48 hr hypoxia.

(D) Under the same conditions, combined knockdown of PYGL and p53 prevented cell growth arrest observed with PYGL knockdown only. Mean ± SEM of three independent experiments is shown (*$p < 0.05$). See also Figures S4 and S5.

lysosomes, we detected an increase in fluorescent vacuoles, especially in hypoxia (Figure 5D). In support of this observation, TEM images also revealed an accumulation of vacuoles in the cytosol of PYGL-depleted U87 cells, as compared to normoxia and control cells in hypoxia (Figure 5D). Finally, we also detected increased expression levels of *GAA*, consistent with increased lysosomal activity in PYGL-depleted cells (Figure 5E). Taken together, our data indicate that PYGL depletion results in elevated glycogen accumulation in hypoxia and reduced proliferation due to p53-induced premature senescence.

To further examine the relationship between glycogen accumulation and induction of senescence in PYGL-depleted cells, we analyzed the phenotypic consequences of simultaneous GYS1 and PYGL knockdown. Because GYS1 knockdown was detrimental to MCF-7 and HCT116 cells (Figure S5A) but better tolerated in U87 cells (Figure S5C), we performed the GYS1 and PYGL codepletion studies in this cell line only (Figure S5B). We observed that GYS1 depletion, either alone or in conjunction with the simultaneous knockdown of PYGL, significantly attenuated (but did not completely prevent) glycogen accumulation that normally occurs in hypoxia (Figure S5C). Furthermore, GYS1 and PYGL codepleted cells did not exhibit any cell growth defects in hypoxia, suggesting that a reduction in GYS1-dependent glycogen accumulation ameliorates the premature senescence phenotype normally associated with PYGL knockdown (Figure S5C). Taken together, we propose that glycogen

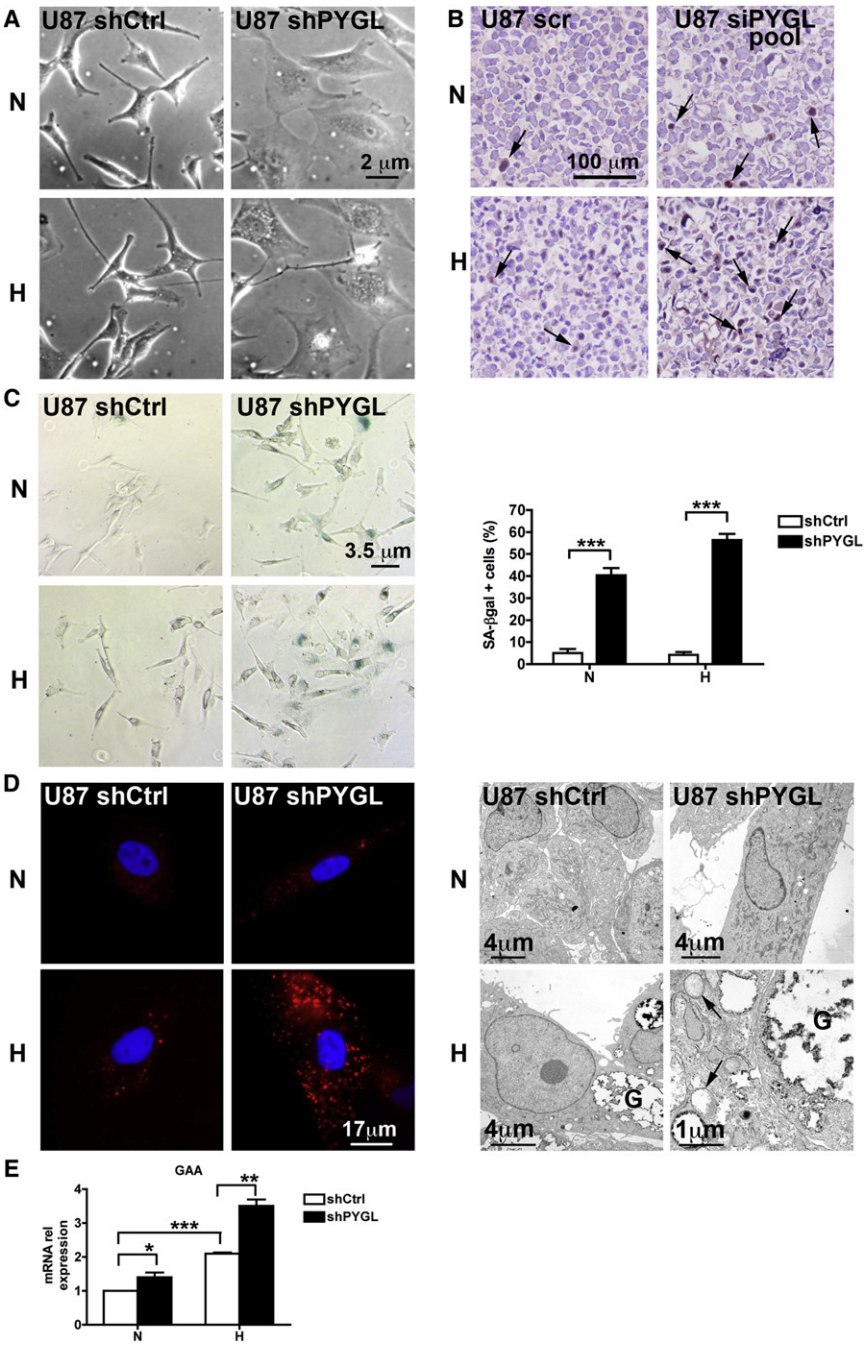

Figure 5. PYGL Knockdown Promotes Senescence

(A) Representative images of U87 cells cultivated in normoxia (N) or hypoxia (H) for 48 hr, displaying senescence-like morphology when PYGL is decreased.

(B) Immunohistochemical analysis of DEC1 in sections of U87 cells treated as in (A). Arrows indicate representative positive cells.

(C) Senescence-associated β-galactosidase staining at pH 6 of U87 shCtrl and shPYGL cells treated as in (A). Senescent cells are colored in blue upon X-gal staining (left panels). Senescence in each condition was quantified and expressed as percentage of SA-β-gal-positive cells (right panel). Mean expression ± SEM of three independent experiments is shown (***$p < 0.001$).

(D) PYGL deficiency was associated with accumulation of lysosomes as shown by LysoTracker red staining, and vacuoles as shown by TEM (arrows). On the left panels, nuclei were stained with DAPI. G, glycogen.

(E) mRNA expression of lysosomal GAA was measured in U87 cells with decreased PYGL levels and compared to control cells in normoxia or after 48 hr at 0.1% O_2. Mean ± SEM of three independent experiments is shown (*$p < 0.05$, **$p < 0.01$, ***$p < 0.001$). See also Figures S4 and S5.

accumulation is required for inhibition of tumor progression in PYGL knockdown cells. We note, however, that low levels of GYS1 and PYGL (due to incomplete knockdown) may still be sufficient for glycogen turnover in U87 cells.

Reactive Oxygen Species Contribute to Premature Senescence in the Absence of PYGL

Next, we examined the specific cause of premature senescence in PYGL-depleted cells. Because ROS are recognized contributors to premature senescence (Kuilman et al., 2010; Lu and Finkel, 2008), we measured the production of mitochondrial superoxide in U87 and MCF-7 cells. Both cell lines showed a marked increase in superoxide levels upon transfection of siPYGL pool (50% ± 6% versus 33% ± 1% in U87 and 33% ± 4% versus 17% ± 0.5% in MCF-7) (Figure 6A). When cells were simultaneously exposed to the cell-permeant ROS scavenger manganese (III) tetrakis (1-methyl-4-pyridyl) porphyrin (MnTMPyP), the production of superoxide was significantly reduced in both control and siPYGL pool cells (Figure 6B). Moreover, intracellular ROS, as measured by generation of dichlorofluoresceine (DCF) from 2′, 7′-dichloro-dihydrofluoresceine (H2-DCFDA), showed a significant higher level in U87 shPYGL cells, as compared to control cells (Figure 6C). The reduced cell proliferation phenotype normally associated with PYGL depletion was also partially suppressed when cells were treated with MnTMPyP (Figure 6D). We therefore propose that increased ROS levels contribute to p53-dependent induction of senescence in PYGL-depleted cells.

Breakdown of glycogen by GP causes the release of G1P that is then converted to G6P by the enzyme phosphoglucomutase, and enters the glycolytic cascade or the PPP (Roach et al., 2012). Metabolism of G6P through the PPP is used to generate nucleotides required for sustained proliferation, as well as NADPH, which is an important reducing agent for nucleotide, amino acid, and lipid synthesis, and also for ROS

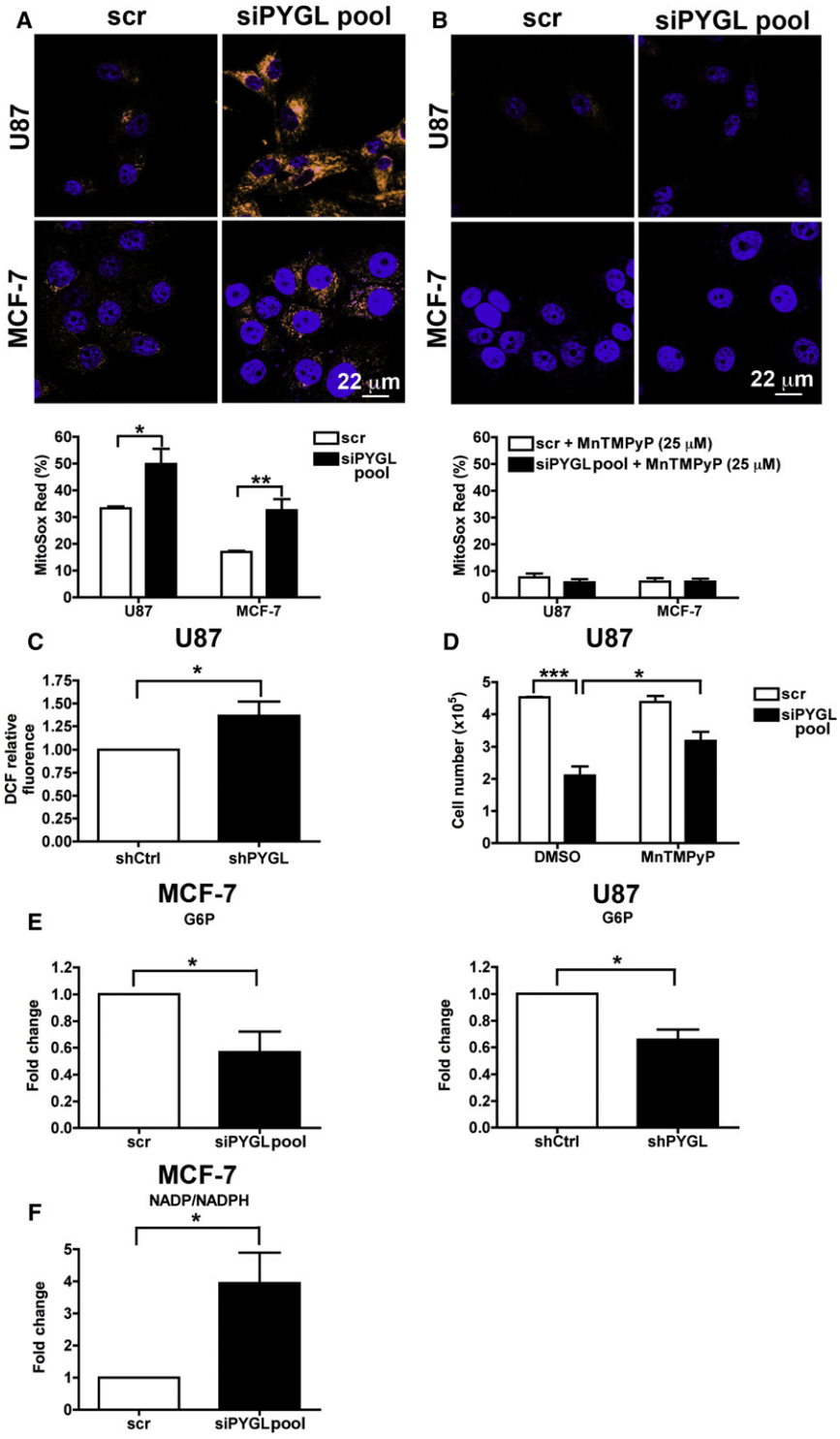

Figure 6. Effects of PYGL Depletion on ROS Accumulation

(A) Transfection of U87 and MCF-7 cells with siPYGL in normoxia significantly increases the levels of mitochondrial superoxide compared to scr-transfected cells, as measured by MitoSox Red staining. Representative confocal images are shown on the top panels, and quantification by flow cytometry is shown on the bottom panel. Mean ± SEM of three independent experiments is shown (*$p < 0.05$, **$p < 0.01$).

(B) Superoxide accumulation induced by PYGL depletion is abolished in the presence of the superoxide dismutase mimetic MnTMPyP. Cells where cultivated in the presence of 25 μM MnTMPyP/DMSO for 48 hr after transfection. Mean expression ± SEM of three independent experiments is shown.

(C) DCF accumulation at 48 hr in normoxia, induced by PYGL depletion in U87 cells. Mean ± SEM of three independent experiments is shown (*$p < 0.05$).

(D) The decrease in cell number induced by PYGL knockdown in U87 cells is partially rescued when MnTMPyP is added to the cells. Mean ± SEM of three independent experiments is shown (*$p < 0.05$, ***$p < 0.001$).

(E) PYGL loss results in decreased levels of G6P in MCF-7 and U87 cells. Cells were cultivated in normoxia for 48 hr before analysis. Mean ± SEM of three independent experiments is shown (*$p < 0.05$).

(F) Depletion of PYGL is associated with increased $NADP^+$/NADPH ratio. MCF-7 cells were treated as in (E). Mean ± SEM of three independent experiments is shown (*$p < 0.05$). See also Figures S5 and S6 and Table S2.

scavenging (Lunt and Vander Heiden, 2011). Because the depletion of PYGL was associated with an increase in ROS and an arrest in proliferation, we hypothesized that the PPP could be affected by the inability to metabolize glycogen in the absence of PYGL. We observed a significant reduction of G6P levels in PYGL-depleted cells (Figure 6E). This was associated with a significant increase in the $NADP^+$/NADPH ratio in MCF-7 cells upon transfection with siPYGL pool (Figure 6F). Furthermore, our hypothesis that the PPP activity is affected by reduced G6P levels in PYGL-depleted cells was confirmed by flux analysis with D-[1,2-^{13}C]glucose, which showed reduced ^{13}C incorporation in a position in ribose in adenosine and guanosine nucleotides that is unique to oxidative PPP (Figures S5D–S5F). To confirm that reduced PPP activity is associated with increased cell senescence, we treated U87 cells with two specific PPP inhibitors, 6-aminonicotinamide (6-AN) and dehydroepiandrosterone (DHEA) (Polimeni et al., 2011). We observed that treatment with either of these agents induced a significant increase in the proportion of senescent cells (Figure S5G). We conclude that PYGL depletion impairs the PPP pathway, due to a reduction in intracellular G6P and hence NADPH levels.

In order to obtain a more comprehensive overview of the metabolic changes induced by PYGL depletion (Figure S6B),

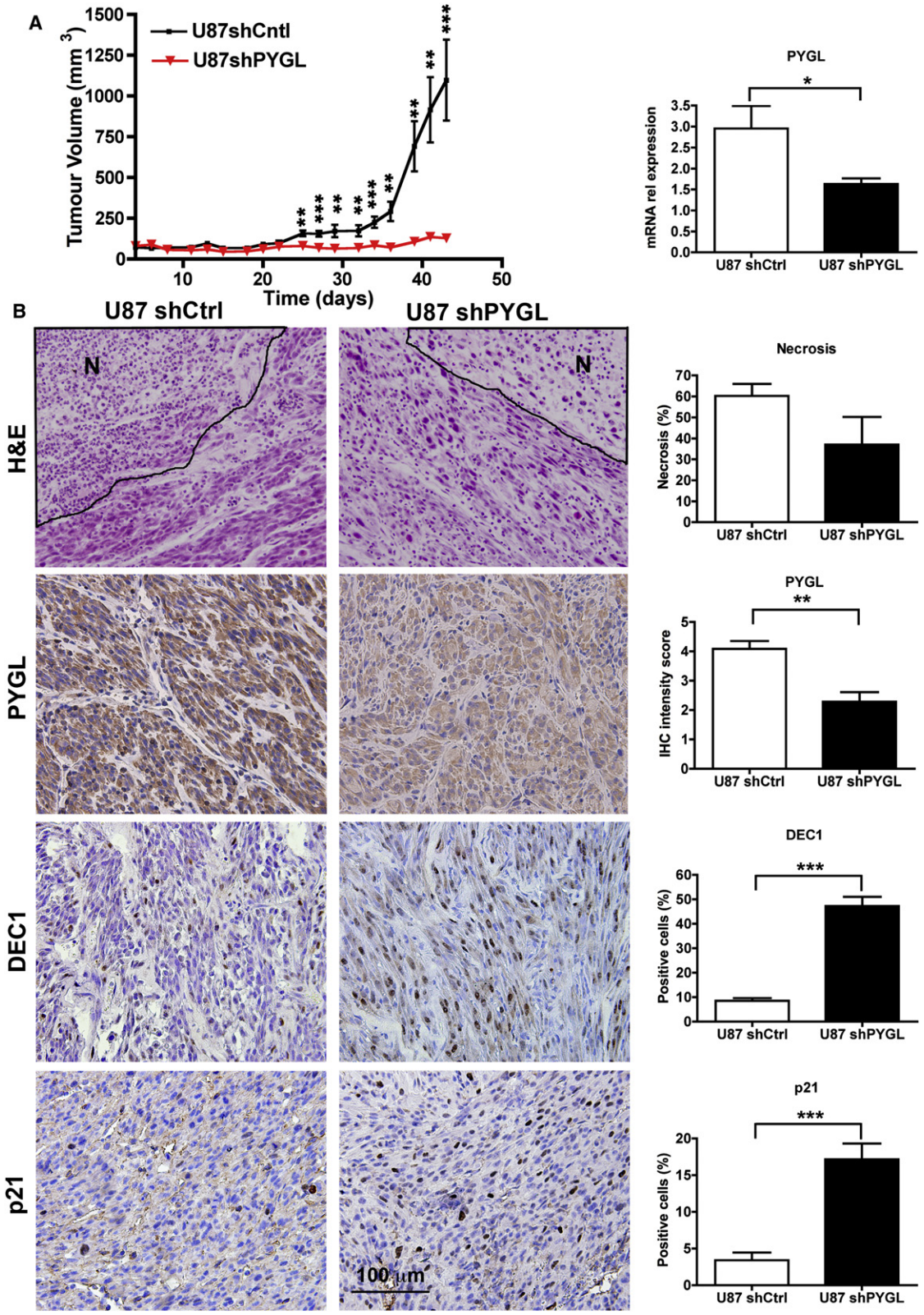

Figure 7. PYGL Knockdown Impairs Tumor Growth and Triggers Senescence

(A) PYGL knockdown in U87 cells significantly reduced tumor growth compared to control cells (left panel). 10^7 U87 shCtrl or U87 shPYGL cells were injected subcutaneously in BALB/c nu/nu mice. Tumor volumes were measured every 3 days. Points represent the average size ±SEM of five to seven tumors (**p < 0.01,

we then performed metabolic profiling of MCF-7 siPYGL pool versus control cells using gas chromatography-mass spectrometry (GC-MS) and liquid chromatography-tandem mass spectrometry (LC-MS/MS) (Table S2 and Figure S6A). Consistent with a pattern of decreased flux of G6P through the PPP and increased ROS levels, PYGL knockdown cells exhibited lower levels of 6-phosphogluconate and nucleotides, and increased levels of oxidized glutathione (GSSG). The evaluation of extracellular glucose and lactate did not show any significant difference between PYGL knockdown and control cells (Figure S6B).

Taken together, our data suggest that PYGL is required to sustain cancer cell proliferation, and its absence leads to increased ROS-induced premature senescence. Furthermore, we propose that attenuation of glycogen breakdown by PYGL depletion leads to decreased levels of G6P and NADPH, which impair nucleotide production and ROS scavenging potential (Figure S6C).

PYGL Knockdown Impairs the In Vivo Growth of Tumor Xenografts

Next, we tested the effect of PYGL depletion in spheroids as a 3D model of cancer cell growth. Both U87 and MCF-7 cells formed spheroids. After 7 days from plating, spheroid volumes were markedly reduced in the siPYGL pool group ($8.8 \pm 1.3 \times 10^7$ versus $27.0 \pm 0.7 \times 10^7$ μm^3 for U87 and $6.8 \pm 1.0 \times 10^7$ versus $11.6 \pm 0.0 \times 10^7$ μm^3 for MCF-7) (Figure S7A). Growth was also significantly reduced in spheroids derived from U87 cells with stable PYGL knockdown, and this was associated with increased glycogen levels, as measured by PAS staining (Figure S7B).

To test the in vivo roles of PYGL during cancer development, U87 cells with stable PYGL knockdown or U87 control cells were injected subcutaneously in nude mice, and tumor growth was monitored. PYGL depletion resulted in a profound reduction of tumor growth as compared to controls. In particular, at day 43 after injection, tumor volumes were $1,095 \pm 250$ versus 130 ± 25 mm^3 in the control and the PYGL knockdown groups, respectively (Figure 7A). In vitro, we observed that PYGL depletion impaired cell proliferation via the induction of senescence. To investigate whether a similar mechanism was responsible for tumor growth inhibition in vivo, tumors were collected at the end of the experiment (day 43) and examined for the senescence-associated markers DEC1 and p21. PYGL reduction was associated with a significant 5-fold increase in the expression of both DEC1 ($47.2\% \pm 3.8\%$ versus $8.5\% \pm 1.1\%$) and p21 ($17.2\% \pm 2.1\%$ versus $3.4\% \pm 1.1\%$) (Figure 7B). Importantly, U87 knockdown and control tumors had similar levels of necrosis, excluding the possibility that this type of cell death was contributing to tumor growth suppression in vivo (Figure 7B). These results suggest that PYGL represents a strong candidate for anticancer therapy.

DISCUSSION

Glycogen metabolism has recently been proposed as an important pathway of metabolic reprogramming in cancer cells (Brahimi-Horn et al., 2011; Pelletier et al., 2012; Pescador et al., 2010; Shen et al., 2010). In this study, we demonstrated an essential role of glycogen breakdown in cancer cells. More specifically, we report that depletion of the catabolic enzyme PYGL resulted in glycogen accumulation that was associated with reduced proliferation and a corresponding induction of senescence. Our data highlight how a greater understanding of cellular metabolism reprogramming events during tumor development can reveal which specific metabolic pathways comprise putative targets for anticancer therapies.

Consistent with altered glycogen turnover being a feature of hypoxia, we observed upregulation of a number of enzymes implicated in glycogen metabolism in vivo. The coordinated induction of these enzymes suggests that glycogen metabolism is functionally associated with cellular adaptation to hypoxia. As part of our analyses, we observed characteristic signatures of GYS1 and PYGL induction, as well as glycogen accumulation, in response to hypoxia. Moreover, our data were consistent with an acute induction of glycogen synthesis catalyzed by GYS1, followed by a subsequent induction of PYGL-dependent breakdown of glycogen. Our results provide a more comprehensive analysis of the glycogen metabolism profile in hypoxia as compared to a previous study in which only the early anabolic response (up to 24 hr) was reported (Pescador et al., 2010).

The phenotypic consequences of disrupting glycogen breakdown were surprisingly profound, both in vitro and in vivo. This suggests that the channeling of glucose through glycogen has important implications for cell growth, and that glycogen may possess additional physiological functions that go beyond its role as an energy source in situations of increased glucose demand. A similar phenomenon, whereby glucose is incorporated into glycogen and subsequently released as G1P even in the presence of abundant extracellular glucose, has been described previously in brain astrocytes, and is referred to as the "glycogen shunt" (Obel et al., 2012). However, the precise reasons for this physiological response remain largely unexplained.

We propose that the enhanced induction of senescence following PYGL depletion occurs, at least partly, via a ROS-dependent mechanism that leads to the activation of p53. Evidence for this comes from our observations that the premature senescence phenotype associated with PYGL knockdown could be partially suppressed by codepleting p53, or by adding a ROS scavenger. Future studies will aim to test this hypothesis also in vivo. Our flux and metabolomic analyses also revealed that PYGL depletion led to reduced flux through the PPP, which is important for generating NADPH, nucleotides, amino acids, and lipids required for continued cell proliferation. A number of

***$p < 0.001$). At the end of the experiment, PYGL mRNA expression was analyzed in the two groups (right panel). Mean ± SEM of five to seven tumors is shown (*$p < 0.05$).

(B) From top to bottom: tumor histology with necrotic areas indicated by N, persistence of knockdown was determined by immunostaining for PYGL, tumor cell senescence was measured by staining for DEC1 and p21. Representative images are shown on the left, quantification is displayed on the right. For quantification, three to six fields of each tumor sample at 200× magnification were analyzed. Mean expression ±SEM of five to seven tumors is shown (**$p < 0.01$, ***$p < 0.001$). See also Figure S7.

other studies have verified the importance of GP in sustaining continued cell proliferation. Inhibition of GP using a small molecule inhibitor (CP-320626) promoted apoptosis by limiting glucose oxidation, nucleic acid, and lipid synthesis in a human pancreatic cancer cell line (Lee et al., 2004). More recently, activation of various stress-induced pathways and increased levels of cell-cycle regulators were also reported (Ma et al., 2012). A similar effect on cell viability was reported in human umbilical endothelial cells treated with escalating doses of CP-320626 (Vizán et al., 2009). However, the specificity of these results remains to be determined, in view of the considerably higher (more than 1,000-fold) IC_{50} reported by the authors, compared to the one previously determined on purified enzyme (Oikonomakos et al., 2002). Moreover, glycogen accumulation after GP inhibition was not measured.

Notably, we cannot exclude the possibility that glycogen itself fulfils important intracellular signaling functions, at least when present at high levels. Consistent with this possibility, the induction of senescence in PYGL-depleted cells was also suppressed by preventing GYS1-dependent glycogen accumulation. The putative signaling functions of glycogen may arise through its ability to directly regulate the activity of AMP-activated protein kinase (AMPK) (McBride et al., 2009), which can lead to p53-dependent cellular senescence if persistently activated (Jones et al., 2005).

Collectively, we propose that glycogen degradation by PYGL provides a source of G6P (which can maintain the reduction of NADPH and glutathione, and the synthesis of nucleotides, through the PPP) and limits the intracellular levels of glycogen (that may otherwise directly contribute to the induction of senescence). Therefore, in hypoxic cells lacking PYGL, glycogen accumulation, decreased nucleotide synthesis, and increased levels of ROS may all additively contribute to a p53-dependent growth arrest (Figure S6C).

Taken together with our promising results obtained in vivo, in which tumorigenesis of U87 shPYGL xenografts was significantly impaired and tumor senescence was induced, a number of observations have suggested that PYGL may comprise a target for anticancer therapy. First, *PYGL* is one of the 99 genes included in the hypoxia "metagene" that is proposed to form a hypoxic signature with prognostic significance in HNSCC and breast cancer (Winter et al., 2007). Furthermore, our Oncomine search revealed increased expression of *PYGL* in a number of tumor types as compared to normal tissues. Importantly, targeting of PYGL for cancer therapy would likely present limited side effects, because patients affected by Hers disease, an inherited glycogen storage disease caused by deficiency of PYGL, present only mild symptoms during childhood, and most adults are asymptomatic (Dagli and Weinstein, 1993). Indeed, small molecule inhibitors of PYGL are currently under investigation for the treatment of diabetes (Praly and Vidal, 2010). Our data suggest that these could also warrant consideration as possible anticancer therapies in future studies. In particular, given that PYGL expression is increased following bevacizumab treatment in vivo, we predict that targeting of this pathway is likely to be more effective in tumors that are markedly hypoxic. It will be of great interest to investigate the combined effects of PYGL inhibition and bevacizumab and to determine if PYGL is required for resistance to antiangiogenic therapy.

EXPERIMENTAL PROCEDURES

Cell Culture

The glioblastoma U87, breast cancer MCF-7, and colon cancer HCT116 cell lines were provided by Cancer Research UK Cell Services and were grown in high-glucose (25 mM) Dulbecco's modified Eagle's medium (DMEM) supplemented with 10% fetal bovine serum. In a set of experiments, U87 cells were cultivated in low glucose (5 mM) DMEM (GIBCO-BRL). Cell exposure to hypoxia (0.1% oxygen) was undertaken in an in $vivo_2$ 400 hypoxic workstation (Ruskinn Technologies).

Glycogen Quantification

Glycogen levels were measured using the Glycogen Assay Kit (BioVision) following manufacturer's instructions. Briefly, cells were homogenized with 200 μl of dH_2O on ice and then boiled for 5 min. Homogenates were spun at 13,000 rpm for 5 min and supernatants were assayed for glycogen content. Results were normalized by protein content or cell number.

Periodic Acid Schiff Staining

Glycogen was detected in cells, spheroids, and tumor sections following a standardized periodic acid Schiff (PAS) staining technique. Briefly, cells were fixed with 4% paraformaldehyde for 15 min, incubated in 1% periodic acid (Sigma-Aldrich) for 5 min, rinsed in water, and placed in Schiff's reagent (Sigma-Aldrich) for 10 min. Finally, cells were washed with water. Amylase (Sigma-Aldrich) was used in a set of experiments to verify that staining was specific for glycogen. Images were obtained using a Zeiss Axiovert 135 microscope.

Electron Microscopy

Cell pellets were fixed in 4% glutaraldehyde in 0.1 M phosphate buffer and processed for routine electron microscopy (Ling et al., 2006). In summary, the samples were postfixed in osmium tetroxide, dehydrated in ethanol, treated with propylene oxide, and embedded in Spurr's epoxy resin. Sections (1 μm) were stained with Azure A for light microscopy and thin sections stained with uranyl acetate and lead citrate prior to examination in a Jeol 1200EX electron microscope. Specific staining for polysaccharides was carried out using an adaptation of the PATO method (Ferguson et al., 1977).

Sa-β-Gal Staining

To detect senescent cells, a Senescence Detection Kit (Calbiochem) was used, and staining was performed according to manufacturer's instructions. Images were acquired with a Zeiss Axiovert 135 microscope.

Cell-Cycle Analysis

To evaluate cell-cycle distribution, cells were washed with ice-cold PBS, resuspended in 1 ml of PBS, and fixed by the dropwise addition of 3 ml of 100% ethanol for 20 min at 4°C. Cells were washed twice with ice-cold PBS and resuspended in a PI solution (100 μg/ml) containing DNase-free RNase (12 μg/ml) (Sigma). After 15 min incubation at room temperature, cells were analyzed in a FACS analyzer Cyan ADP (Dako).

ROS Detection

ROS levels were measured using either MitoSOX Red (Molecular Probes), as an indicator of mitochondrial superoxide, or H2-DCFDA (Molecular Probes), as an indicator of intracellular ROS. Cells were treated as appropriate and subsequently loaded with 5 μM MitoSOX Red or H2-DCFDA for 45 min. For microscopic analysis, cells were washed with PBS and mounted with Vecta-Shield (Vector Laboratories) with DAPI. Images were acquired with a Zeiss Axioskop 2 plus microscope. For flow cytometry analysis, cells were washed and scraped in PBS and immediately analyzed in a FACS analyzer Cyan ADP. In a set of experiments, cells were cultivated in the presence of 25 μM MnTMPyP (Calbiochem).

Glucose-6-Phosphate and $NADP^+$/NADPH Quantification

G6P levels and $NADP^+$/NADPH ratio were determined with the Glucose-6-Phosphate Assay Kit and the $NADP^+$/NADPH Quantification Kit (both from BioVision), respectively. Measurements were performed according to the

manufacturer's instruction. Results were presented as fold change in MCF-7 siPYGL pool versus MCF-7 scr.

Mouse Tumor Studies

All protocols were carried out under Home Office regulations (Li et al., 2007). Six- to eight-week-old female BALB/c SCID or BALB/c NuNu mice (Harlan Sprague Dawley, Inc.) were injected subcutaneously in the lower flank with 100 μl of Matrigel (BD Bioscience) and 1×10^7 cells suspended in 100 μl of serum-free medium. Tumor growth was monitored and measured three times per week using calipers. Tumor volume was calculated from the formula $V = L \times W \times H \times \pi/6$ (L = length, W = width, and H = height). When tumors reached 1.44 cm^3, mice were sacrificed by cervical dislocation. Ninety minutes prior to sacrifice, mice were injected intraperitoneally with 100 mg/kg of pimonidazole (Hypoxyprobe-1; Chemicon International).

Tumor samples at different stages of development from the Her-2/neu transgenic spontaneous mouse model of breast carcinogenesis were kindly provided by S. Indraccolo (IOV-IRCCS, Padua, Italy).

Histology and Immunohistochemistry

A standard hematoxylin and eosin protocol was followed to assess the morphology of HCT116 spheroids. Immunohistochemistry was carried out as previously described (Li et al., 2007). The following primary antibodies were used: pimonidazole (Hypoxyprobe-1; Chemicon International), GYS1 (abcam), PYGL (Sigma-Aldrich), DEC1 (CW27), p21 (Dako), CA9 (M75). Slides were incubated with the anti-rabbit/anti-mouse secondary antibody (Dako), and DAB (Dako) was applied to the sections for 5–8 min. The slides were counterstained by immersing in hematoxylin solution (Sigma-Aldrich) and mounted with Aquamount (VWR). Slides were scored by two researchers blinded to grouping or analyzed quantitatively by image analysis in ImageJ using color deconvolution as described previously (Ruifrok and Johnston, 2001).

Statistical Analyses

Statistical analysis and graphs were performed using GraphPad Prism v4.0b software (GraphPad). Statistics were carried out using Student's t tests and linear regression of log-transformed growth data. Results are means + SEM, and significance is represented by $^*p < 0.05$, $^{**}p < 0.01$, and $^{***}p < 0.001$.

SUPPLEMENTAL INFORMATION

Supplemental Information includes seven figures, two tables, Supplemental Experimental Procedures, and Supplemental References and can be found with this article at http://dx.doi.org/10.1016/j.cmet.2012.10.017.

ACKNOWLEDGMENTS

The authors would like to thank Hocine W. Mankouri for helpful discussion and critical review of the manuscript. The authors are grateful to Stefano Indraccolo for providing samples of the Her-2/neu transgenic mouse model. This study was supported by GlaxoSmithKline, the University of Oxford, CRUK, the EU 6th and 7th Framework Programs, the Breast Cancer Research Foundation, the Oxford National Institute for Health Research Comprehensive Biomedical Research, the Oxford CRUK Cancer Centre, and the EU METAFLUX grant.

Received: May 22, 2012
Revised: September 9, 2012
Accepted: October 24, 2012
Published online: November 21, 2012

REFERENCES

Berg, J.M., Tymoczko, J.L., and Stryer, L. (2002). Biochemistry (New York: W.H. Freeman).

Bouskila, M., Hunter, R.W., Ibrahim, A.F., Delattre, L., Peggie, M., van Diepen, J.A., Voshol, P.J., Jensen, J., and Sakamoto, K. (2010). Allosteric regulation of glycogen synthase controls glycogen synthesis in muscle. Cell Metab. *12*, 456–466.

Brahimi-Horn, M.C., Bellot, G., and Pouysségur, J. (2011). Hypoxia and energetic tumour metabolism. Curr. Opin. Genet. Dev. *21*, 67–72.

Collado, M., Gil, J., Efeyan, A., Guerra, C., Schuhmacher, A.J., Barradas, M., Benguría, A., Zaballos, A., Flores, J.M., Barbacid, M., et al. (2005). Tumour biology: senescence in premalignant tumours. Nature *436*, 642. http://dx.doi.org/10.1038/436642a.

Dagli, A.I., and Weinstein, D.A. (1993). Glycogen storage disease type VI. In GeneReviews, R.A. Pagon, T.D. Bird, C.R. Dolan, K. Stephens, and M.P. Adam, eds. (Seattle: University of Washington).

el-Deiry, W.S., Tokino, T., Velculescu, V.E., Levy, D.B., Parsons, R., Trent, J.M., Lin, D., Mercer, W.E., Kinzler, K.W., and Vogelstein, B. (1993). WAF1, a potential mediator of p53 tumor suppression. Cell *75*, 817–825.

Ferguson, D.J., Birch-Andersen, A., Hutchison, W.M., and Siim, J.C. (1977). Cytochemical electron microscopy on polysaccharide granules in the endogenous forms of Eimeria brunetti. Acta Pathol. Microbiol. Scand. [B] *85*, 241–248.

Johnson, L.N. (1992). Glycogen phosphorylase: control by phosphorylation and allosteric effectors. FASEB J. *6*, 2274–2282.

Jones, R.G., Plas, D.R., Kubek, S., Buzzai, M., Mu, J., Xu, Y., Birnbaum, M.J., and Thompson, C.B. (2005). AMP-activated protein kinase induces a p53-dependent metabolic checkpoint. Mol. Cell *18*, 283–293.

Kuilman, T., Michaloglou, C., Mooi, W.J., and Peeper, D.S. (2010). The essence of senescence. Genes Dev. *24*, 2463–2479.

Kurz, D.J., Decary, S., Hong, Y., and Erusalimsky, J.D. (2000). Senescence-associated (beta)-galactosidase reflects an increase in lysosomal mass during replicative ageing of human endothelial cells. J. Cell Sci. *113*, 3613–3622.

Lawrence, J.C., Jr., and Roach, P.J. (1997). New insights into the role and mechanism of glycogen synthase activation by insulin. Diabetes *46*, 541–547.

Lee, W.N., Guo, P., Lim, S., Bassilian, S., Lee, S.T., Boren, J., Cascante, M., Go, V.L., and Boros, L.G. (2004). Metabolic sensitivity of pancreatic tumour cell apoptosis to glycogen phosphorylase inhibitor treatment. Br. J. Cancer *91*, 2094–2100.

Li, J.L., Sainson, R.C., Shi, W., Leek, R., Harrington, L.S., Preusser, M., Biswas, S., Turley, H., Heikamp, E., Hainfellner, J.A., and Harris, A.L. (2007). Delta-like 4 Notch ligand regulates tumor angiogenesis, improves tumor vascular function, and promotes tumor growth in vivo. Cancer Res. *67*, 11244–11253.

Ling, Y.M., Shaw, M.H., Ayala, C., Coppens, I., Taylor, G.A., Ferguson, D.J., and Yap, G.S. (2006). Vacuolar and plasma membrane stripping and autophagic elimination of Toxoplasma gondii in primed effector macrophages. J. Exp. Med. *203*, 2063–2071.

Lu, T., and Finkel, T. (2008). Free radicals and senescence. Exp. Cell Res. *314*, 1918–1922.

Lunt, S.Y., and Vander Heiden, M.G. (2011). Aerobic glycolysis: meeting the metabolic requirements of cell proliferation. Annu. Rev. Cell Dev. Biol. *27*, 441–464.

Ma, D., Wang, J., Zhao, Y., Lee, W.N., Xiao, J., Go, V.L., Wang, Q., Recker, R.R., and Xiao, G.G. (2012). Inhibition of glycogen phosphorylation induces changes in cellular proteome and signaling pathways in MIA pancreatic cancer cells. Pancreas *41*, 397–408.

Mamedova, L.K., Shneyvays, V., Katz, A., and Shainberg, A. (2003). Mechanism of glycogen supercompensation in rat skeletal muscle cultures. Mol. Cell. Biochem. *250*, 11–19.

McBride, A., Ghilagaber, S., Nikolaev, A., and Hardie, D.G. (2009). The glycogen-binding domain on the AMPK beta subunit allows the kinase to act as a glycogen sensor. Cell Metab. *9*, 23–34.

Mole, D.R., Blancher, C., Copley, R.R., Pollard, P.J., Gleadle, J.M., Ragoussis, J., and Ratcliffe, P.J. (2009). Genome-wide association of hypoxia-inducible factor (HIF)-1alpha and HIF-2alpha DNA binding with expression profiling of hypoxia-inducible transcripts. J. Biol. Chem. *284*, 16767–16775.

Newgard, C.B., Hwang, P.K., and Fletterick, R.J. (1989). The family of glycogen phosphorylases: structure and function. Crit. Rev. Biochem. Mol. Biol. *24*, 69–99.

Obel, L.F., Müller, M.S., Walls, A.B., Sickmann, H.M., Bak, L.K., Waagepetersen, H.S., and Schousboe, A. (2012). Brain glycogen-new perspectives on its metabolic function and regulation at the subcellular level. Front Neuroenergetics *4*, 3.

Oikonomakos, N.G., Zographos, S.E., Skamnaki, V.T., and Archontis, G. (2002). The 1.76 Å resolution crystal structure of glycogen phosphorylase B complexed with glucose, and CP320626, a potential antidiabetic drug. Bioorg. Med. Chem. *10*, 1313–1319.

Pelletier, J., Bellot, G., Gounon, P., Lacas-Gervais, S., Pouysségur, J., and Mazure, N.M. (2012). Glycogen synthesis is induced in hypoxia by the hypoxia-inducible factor and promotes cancer cell survival. Front Oncol. *2*, 18.

Pescador, N., Villar, D., Cifuentes, D., Garcia-Rocha, M., Ortiz-Barahona, A., Vazquez, S., Ordoñez, A., Cuevas, Y., Saez-Morales, D., Garcia-Bermejo, M.L., et al. (2010). Hypoxia promotes glycogen accumulation through hypoxia inducible factor (HIF)-mediated induction of glycogen synthase 1. PLoS ONE *5*, e9644. http://dx.doi.org/10.1371/journal.pone.0009644.

Polimeni, M., Voena, C., Kopecka, J., Riganti, C., Pescarmona, G., Bosia, A., and Ghigo, D. (2011). Modulation of doxorubicin resistance by the glucose-6-phosphate dehydrogenase activity. Biochem. J. *439*, 141–149.

Praly, J.P., and Vidal, S. (2010). Inhibition of glycogen phosphorylase in the context of type 2 diabetes, with focus on recent inhibitors bound at the active site. Mini Rev. Med. Chem. *10*, 1102–1126.

Ring, D.B., Johnson, K.W., Henriksen, E.J., Nuss, J.M., Goff, D., Kinnick, T.R., Ma, S.T., Reeder, J.W., Samuels, I., Slabiak, T., et al. (2003). Selective glycogen synthase kinase 3 inhibitors potentiate insulin activation of glucose transport and utilization in vitro and in vivo. Diabetes *52*, 588–595.

Roach, P.J., Cheng, C., Huang, D., Lin, A., Mu, J., Skurat, A.V., Wilson, W., and Zhai, L. (1998). Novel aspects of the regulation of glycogen storage. J. Basic Clin. Physiol. Pharmacol. *9*, 139–151.

Roach, P.J., Depaoli-Roach, A.A., Hurley, T.D., and Tagliabracci, V.S. (2012). Glycogen and its metabolism: some new developments and old themes. Biochem. J. *441*, 763–787.

Rousset, M., Zweibaum, A., and Fogh, J. (1981). Presence of glycogen and growth-related variations in 58 cultured human tumor cell lines of various tissue origins. Cancer Res. *41*, 1165–1170.

Ruifrok, A.C., and Johnston, D.A. (2001). Quantification of histochemical staining by color deconvolution. Anal. Quant. Cytol. Histol. *23*, 291–299.

Schmitt, C.A. (2007). Cellular senescence and cancer treatment. Biochim. Biophys. Acta *1775*, 5–20.

Semenza, G.L. (2002). Involvement of hypoxia-inducible factor 1 in human cancer. Intern. Med. *41*, 79–83.

Shen, G.M., Zhang, F.L., Liu, X.L., and Zhang, J.W. (2010). Hypoxia-inducible factor 1-mediated regulation of PPP1R3C promotes glycogen accumulation in human MCF-7 cells under hypoxia. FEBS Lett. *584*, 4366–4372.

Ursini-Siegel, J., Schade, B., Cardiff, R.D., and Muller, W.J. (2007). Insights from transgenic mouse models of ERBB2-induced breast cancer. Nat. Rev. Cancer *7*, 389–397.

Vigoda, A., Mamedova, L.K., Shneyvays, V., Katz, A., and Shainberg, A. (2003). Glycogen metabolism in rat heart muscle cultures after hypoxia. Mol. Cell. Biochem. *254*, 311–318.

Vizán, P., Sánchez-Tena, S., Alcarraz-Vizán, G., Soler, M., Messeguer, R., Pujol, M.D., Lee, W.N., and Cascante, M. (2009). Characterization of the metabolic changes underlying growth factor angiogenic activation: identification of new potential therapeutic targets. Carcinogenesis *30*, 946–952.

Warburg, O. (1956). On the origin of cancer cells. Science *123*, 309–314.

Ward, P.S., and Thompson, C.B. (2012). Metabolic reprogramming: a cancer hallmark even warburg did not anticipate. Cancer Cell *21*, 297–308.

Winter, S.C., Buffa, F.M., Silva, P., Miller, C., Valentine, H.R., Turley, H., Shah, K.A., Cox, G.J., Corbridge, R.J., Homer, J.J., et al. (2007). Relation of a hypoxia metagene derived from head and neck cancer to prognosis of multiple cancers. Cancer Res. *67*, 3441–3449.

Wykoff, C.C., Beasley, N.J., Watson, P.H., Turner, K.J., Pastorek, J., Sibtain, A., Wilson, G.D., Turley, H., Talks, K.L., Maxwell, P.H., et al. (2000). Hypoxia-inducible expression of tumor-associated carbonic anhydrases. Cancer Res. *60*, 7075–7083.

Zu, X.L., and Guppy, M. (2004). Cancer metabolism: facts, fantasy, and fiction. Biochem. Biophys. Res. Commun. *313*, 459–465.